

Supporting Information

9.7%-Efficient $\text{Sb}_2(\text{S,Se})_3$ Solar Cells with Dithieno[3,2-b:2',3'-d]pyrrol-Cored Hole Transporting Material

Chenhui Jiang,^{a†} Jie Zhou,^{b†} Rongfeng Tang,^a Weitao Lian,^a Xiaomin Wang,^a Xunyong Lei,^c Hualing Zeng,^c Changfei Zhu,^a Weihua Tang^{*b} and Tao Chen^{*a}

^a. Hefei National Laboratory for Physical Sciences at Microscale, CAS Key Laboratory of Materials for Energy Conversion, Department of Materials Science and Engineering, School of Chemistry and Materials Science, University of Science and Technology of China, Hefei, Anhui 230026, P. R. China E-mail: tchenmse@ustc.edu.cn

^b. School of Chemical Engineering, Nanjing University of Science and Technology, Nanjing 210094, China. E-mail: whtang@njust.edu.cn

^c. ICQD, CAS Key Laboratory of Strongly-coupled Quantum Matter Physics, University of Science and Technology of China, Hefei 230026, China

† These authors contributed equally to this work.

Experimental Procedures

Substrate preparation

FTO-coated glass supplied by Advanced Election Technology Co., Ltd., was patterned by laser scribing, followed by ultrasonic cleaning in deionized water, isopropanol, acetone, and ethanol for 30 min, respectively. After drying, the substrate was treated by UV ozone cleaner for 15 min. Chemical bath deposition (65 °C, 18 min) was used to deposit a CdS buffer layer with the thickness of 80 nm.¹ Subsequently, CdS layer was treated with 20 mg mL⁻¹ CdCl₂ absolute methanol solution by spin coating at a speed of 3000 rpm for 30 s, baked on the hotplate at 400 °C for 5 min in air ambient and then cooled down to room temperature naturally.²

Deposition of Sb₂(S,Se)₃ film and device fabrication

The Sb₂(S,Se)₃ film was deposited onto CdS buffer layer by hydrothermal method. Potassium antimony (III) L(+)-tartrate hemihydrate (C₄H₄KO₇Sb·0.5H₂O), sodium thiosulfate pentahydrate (Na₂S₂O₃·5H₂O), and selenourea (CH₄N₂Se) were used as Sb, S, and Se source, respectively. Firstly, 40 mL aqueous solution of C₄H₄KO₇Sb·0.5H₂O (0.2671 g) was stirred until clarification in the inner Teflon tank of autoclave (50 mL). Subsequently, Na₂S₂O₃·5H₂O (0.7942 g) and CH₄N₂Se (0.020 g) were simultaneously added the former solution with stirring and the solution became pale yellow slowly. Then CdS buffer layer coated FTO substrates were immersed into the solution. The autoclave was sealed and kept at 150 °C for 110 minutes to allow the growth of Sb₂(S,Se)₃ film with a thickness of 300 nm on the substrates. The obtained Sb₂(S,Se)₃ films were washed with deionized water and ethanol, followed by drying in a N₂ flow. Finally, the samples were placed in vacuum at 110 °C for 2 minutes, followed by annealing at 350 °C for 10 minutes in N₂-filled glovebox.

For deposition of hole-transport materials, the Spiro-OMeTAD solution was prepared by mixing 36.6 mg of Spiro-OMeTAD, 14.5 μL of 4-tert-butylpyridine (tBP) and 9.5 μL of a lithium bis(trifluoromethanesulfonyl)imide (Li-TFSI) solution in acetonitrile (520 mg/mL) into 1 mL of chlorobenzene. The Spiro-OMeTAD solution with additives was spin-coated onto Sb₂(S,Se)₃ surface at 3000 rpm for 30 s according to the reported method.³ In case of DTPTThMe-ThTPA, optimal 8 mg DTPTThMe-ThTPA was dissolved in 1 mL chloroform, and then 8 μL tBP and 5 μL Li-TFSI solution (520 mg/mL in acetonitrile) were added. The DTPTThMe-ThTPA solution was spin-coated onto Sb₂(S,Se)₃ film at 3000 rpm for 30 s. Eventually, Au counter electrode was deposited through a shadow mask by a thermal evaporator. The active area of the device was defined as 0.09 cm².

Sb₂(S,Se)₃ Film Characterizations

X-ray diffraction (XRD) patterns of samples were performed on a Bruker Advance D8 diffractometer equipped with Cu K α radiation ($\lambda = 1.5416 \text{ \AA}$). The optical characteristics of the films were measured with a UV-visible spectrophotometer (SOLID 3700). The surface, cross sections morphologies and EDS spectra of the samples were examined by SEM (FE-SEM SU 8220). Steady-state photoluminescence (PL) was measured using a LabRamHR system with excitation at 532 nm. Band energies of Sb₂(S,Se)₃ film and XPS were performed by synchrotron radiation photoemission spectroscopy (SRPES) at the National Synchrotron Radiation Laboratory (NSRL) in Hefei, China. By plotting $(Ah\nu)^2$ versus energy ($h\nu$) curve deduced from UV-vis absorption spectroscopy, the band gap ($E_g=1.50 \text{ eV}$) between conduction band edge and the valence band edge for Sb₂(S,Se)₃ film was measured. The work function (W_i)

of related materials were obtained by subtracting the binding energies of the secondary electron cutoffs (E_{SEC}) from the excitation light energy ($h\nu$, 40 eV), denoted as $W_f = h\nu - E_{\text{SEC}}$ (4.41 eV = 40 eV - 35.59 eV). In the valence band (VB) region, the low binding energy tail threshold (E_{VB}) refers to the energy difference between the valence band maximum and Fermi level. Accordingly, the valence band energy level (E_v) was calculated by $E_v = -E_{\text{VB}} - W_f$ (-5.37 eV = -0.96 eV - 4.41 eV). Based on these results and the band gap value, the conduction band energy was determined by $E_c = E_v + E_g$ (-3.87 eV = -5.37 eV + 1.50 eV).⁴ The related energy diagram is shown in **Figure S8d**.

Broadband femtosecond-TA measurements were performed on a pump-probe system (Helios, Ultrafast System LLC) coupled with an amplified femtosecond laser system (Coherent) under ambient conditions. The pulse beam was excited by a Ti:sapphire regenerative amplifier (Legend Elite-1K-HE; pulse width, 35 fs; pulse energy, 7 mJ per pulse; repetition rate, 1 kHz; 800 nm), and seeded with a mode-locked Ti:sapphire laser system (Mica 5) and an Nd:YLF laser (Evolution 30) pumped. This pulse beam was then split into two portions. The larger portion was passed an optical parametric amplifier (TOPAS-800-fs, Coherent) to generate the pump pulse (pulse width, around 100 fs; pulse energy, 0.027 μ J per pulse; repetition rate, 1 kHz; 365 nm). The smaller portion (around 0.1 μ J per pulse) of the 800 nm pulse beam was focused into a sapphire plate to produce the white light continuum (WLC) probe pulse (from 430 nm to 770 nm). The pulse-to-pulse fluctuation of the WLC probe pulse was corrected by a reference beam split from itself. A mechanical chopper operated at a frequency of 500 Hz was used to modulate the pump pulses. The temporal and spectral profiles (chirp-corrected) of the pump-induced differential transmission of the WLC probe light (i.e., absorbance change) were visualized by an optical fiber-coupled multichannel spectrometer (with a CMOS sensor). All the TA data was obtained and averaged from at least 5 scans to ensure the accuracy and high signal-to-noise ratio. TAS decay curves are well fitted with the monoexponential equation (1)⁵:

$$I_t = I_0 \exp\left(-\frac{t}{\tau}\right) + C \quad (1)$$

where I_t and I_0 refer to the TAS intensity at time t and zero, and τ is the carrier lifetime.

Device Characterizations

The J - V curves were recorded using a Keithley 2400 apparatus under solar-simulated AM 1.5 sunlight (100 mW cm^{-2}) with a standard xenon-lamp-based solar simulator (Oriel Sol 3A, Japan). The solar simulator illumination intensity was calibrated by a monocrystalline silicon reference cell (Oriel P/N 91150 V, with KG-5 visible color filter) calibrated by the National Renewable Energy Laboratory (NREL). The external quantum efficiency (EQE, Model SPIEQ200) was measured using a single source illumination system (halogen lamp) combined with a monochromator. Electrochemical impedance spectroscopy (EIS) measurements were performed using Zahner Mess System PP211 electrochemical workstation at a bias potential of 0.50 V in dark with the frequency ranging from 100 Hz to 1 MHz. The obtained impedance spectra were fitted with Z-View software (v2.8b, Scribner Associates, USA). To quantitatively investigate the impact of HTMs on the built-in potential, Mott-Schottky analysis of the capacitance versus voltage curve was conducted by Zahner Mess System PP211 electrochemical workstation at room temperature in darkness at a frequency of 10 kHz and the AC amplitude was 5 mV. DC bias voltage was changed from -0.1 to 1.2 V. The built-in potential is estimated by the X-intercept of Mott-Schottky plot ($1/C^2$ is plotted against the applied voltage V) based on equation (2)⁶:

$$\frac{1}{C^2} = \frac{2}{\epsilon_0 \epsilon_r e A^2 N} (V_{bi} - V) \quad (2)$$

where C is capacitance, A is device area, ϵ_0 is the vacuum dielectric constant, ϵ_r is the relative dielectric constant of the $\text{Sb}_2(\text{S,Se})_3$ films with a value of 5, e is elementary charge, N is carrier concentration and V_{bi} is the built-in potential, respectively. The transient photocurrent delay (Zahner PP211 and Zahner Zennium) was generated by a microsecond pulse of a white light incident without bias light on solar cells under short circuit conditions. The decay time can be well fitted by an exponential equation (3):

$$y = y_0 + Ae^{-x/t} \quad (3)$$

We also investigated the charge recombination kinetics using light intensity-dependent V_{oc} measurement for the various devices according to the following equations (4)⁷:

$$V_{oc} = n \frac{kT}{q} \ln(I) + C \quad (4)$$

where k is the Boltzmann constant, T is absolute temperature, q refers to elementary charge, I is the light intensity, C is a constant, and n is ideal factor related to recombination.

General methods and materials for HTM

¹H and ¹³C NMR spectra were collected from a Bruker Avance III 500 (500 MHz) spectrometer in CDCl_3 solutions. Mass spectra were obtained by Bruker ultrafleXtreme MALDITOF/TOF. The absorption spectra were measured on a UV-Vis spectrophotometer (Evolution 220, Thermo Fisher). The electrochemical cyclic voltammetry (CV) curves were obtained from an electrochemical workstation (CHI760D Chenhua, Shanghai) with Pt as working electrode, Pt slice as counter electrode, and Ag/AgCl electrode as reference electrode in CH_2Cl_2 solution containing HTMs (*n*-Bu₄NPF₆, 0.1 M) at a scan rate of 50 mV s⁻¹. Ferrocene/ferrocenium (Fc/Fc⁺) was used as the internal standard. The HOMO energy levels were calculated by following HOMO = -(4.8+E_{onsetox}) eV. The LUMO energy level was calculated with HOMO and optical bandgap (E_g) in solid state absorption spectra by the formula as: LUMO = HOMO + E_g (eV). Thermogravimetric analysis (TGA) was conducted on TGA/SDTA851E (Mettler Toledo) under N₂ atmosphere at a heating rate of 20 °C min⁻¹ from 50 °C to 800 °C. DSC analysis was performed on PerkinElmer Thermal Analysis from 50 °C to 300 °C with a heating/cooling rate of 10 °C min⁻¹.

Hole Mobility Measurements

Hole mobilities of HTMs were evaluated by the space-charge-limited-current (SCLC) method with a device configuration of ITO/Au/HTMs/Au. The dark J - V curves of the devices were performed on a Keithley 2400 source at ambient conditions. The hole mobility is extracted by fitting the J - V curves using the modified Mott-Gurney law (5)⁸:

$$J = \frac{9}{8} \epsilon_0 \epsilon_r \mu \frac{V^2}{d^3} \quad (5)$$

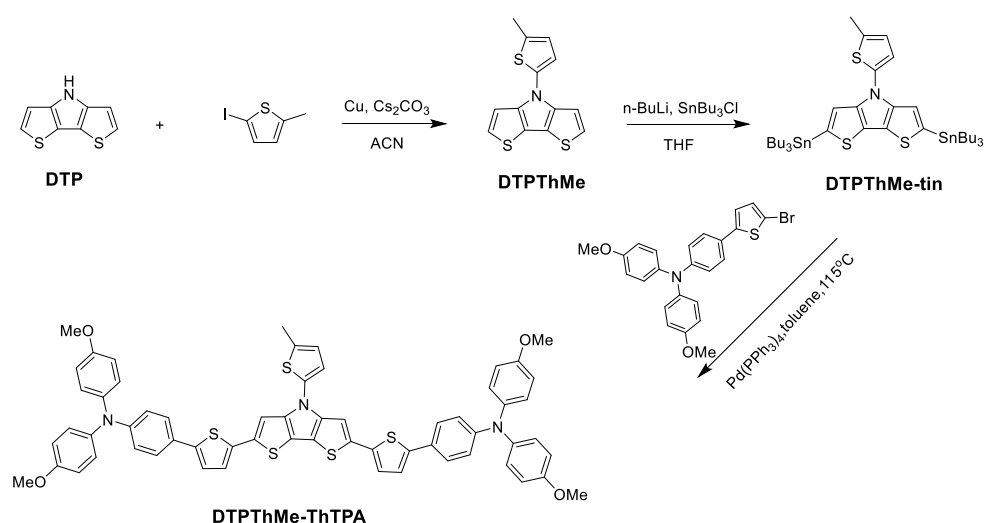
where J is current density, ϵ_0 is the permittivity of free space (8.85×10^{-12} F m⁻¹), ϵ_r is the permittivity of HTM (~3 for organic semiconductors), μ is the hole mobility, V is voltage, and d is film thickness. The thicknesses of Au, Spiro-OMeTAD, and DTPThMe-ThTPA are 60 nm, 80 nm, and 90 nm, respectively.

Quantum chemistry calculations

All calculations were performed using Density Functional Theory (DFT) established in Gaussian09 code. Chemical structural optimization and subsequent frequency calculations were performed for the ground state using an all electron Pople double zeta basis set with one polarization function on heavy atoms (non-hydrogen atoms like C, N, O and S etc.) and one on hydrogen atom (631g(d, p)). The purpose of the frequency calculation is to confirm that there is no imaginary frequency and the optimized chemical structures are at minimum on potential energy surfaces. The hybrid functional B3LYP was used for all these calculations.

Synthesis details for DTPTThMe-ThTPA

Commercially available reagents and dry acetonitrile were purchased from Energy Chemical (Shanghai, China) and used without further purification. Toluene and tetrahydrofuran (THF) were freshly distilled before use. Other solvents were used directly. The synthetic route was depicted in Scheme S1.



Scheme S1. Synthetic Route to DTPTThMe-ThTPA

Synthesis of 4-(5-methylthiophen-2-yl)-4H-dithieno[3,2-b:2',3'-d]pyrrole (DTPTThMe). The suspension of DTP (1.25 g, 6.97 mmol), 2-iodo-5-methylthiophene (2.34 g, 10.46 mmol), Cu power (88.7 mg, 1.39 mmol) and Cs₂CO₃ (6.82 g, 20.92 mmol) in dry acetonitrile (40 mL) was degassed for 30 min with nitrogen bubbling. The reaction mixture was heated to 85 °C and kept stirring until DTP was completely reacted. The mixture was cooled down to room temperature and the solvent was removed under reduced pressure. The crude oil was purified by column chromatography (silica gel, petroleum ether/dichloromethane, v/v, 8/1) to afford DTPTThMe as gray solid (1.15 g, 60 %). ¹H NMR (500 MHz, CDCl₃): 7.16-7.15 (m, 4H), 6.89-6.88 (d, *J* = 3.6 Hz, 1H), 6.69 (d, *J* = 3.6 Hz, 1H), 2.52 (s, 3H); ¹³C NMR (125 MHz, CDCl₃): 139.87, 133.55, 130.22, 118.45, 118.21, 113.81, 111.42, 107.03, 10.32.

Synthesis of 4-(5-methylthiophen-2-yl)-2,6-bis(tributylstannyl)-4H-dithieno[3,2-b:2',3'-d]pyrrole (DTPTThMe-tin) Toward the solution of DTPTThMe (900 mg, 3.27 mmol) in freshly distilled THF (30 mL) at -78 °C was added with n-BuLi (2.88 mL, 7.19 mmol, 2.4 M in hexane) dropwise over 10 min under nitrogen. The reaction mixture was stirred at -78 °C for 1 h, followed by the slow addition of tributyltin chloride (2.45 g, 7.52 mmol). The reaction

mixture was then warmed to room temperature and stirred for another 4 h. The reaction mixture was quenched by KF aqueous solution, extracted with diethyl ether for twice and dried over anhydrous MgSO₄. Compound **2** was obtained after the removal of solvent, which can be directly used in the following step without further purification. ¹H NMR (500 MHz, CDCl₃): 7.13 (s, 2H), 6.90-6.89 (d, *J* = 3.6 Hz, 1H), 6.71-6.70 (d, *J* = 3.6 Hz, 1H), 2.53 (s, 3H).

Synthesis of DTPT_hMe-ThTPA. The solution of DTPT_hMe-tin (525 mg, 0.62 mmol), ThTPA-Br (717 mg, 1.54 mmol) and Pd(PPh₃)₄ (71 mg, 62 μmol) in dry toluene (20 mL) was degassed with nitrogen for 25 min and the mixture was refluxed overnight. After cooling to room temperature and removing the solvent, the crude product was purified by column chromatography (silica gel, petroleum ether/ethyl acetate, v/v, 4/1) to afford target compounds as a red solid (790 mg, 89%). ¹H NMR (500 MHz, CDCl₃): 7.49-7.38 (dd, 4H), 7.19 (s, 2H), 7.11-7.06 (m, 12H), 6.88-6.84 (m, 8H), 6.75-6.74 (dd, 1H), 3.81 (s, 12H), 2.56 (s, 3H); ¹³C NMR (125 MHz, CDCl₃): 156.38, 156.14, 148.37, 140.69, 140.40, 139.20, 136.21, 127.23, 126.81, 126.28, 123.97, 122.42, 120.53, 119.99, 115.59, 114.92, 114.86, 108.03, 55.60, 15.76. MALDI-TOF MS: *m/z*=1045.2181 [M]⁺, calcd. for C₆₁H₄₇N₃O₄S₅: 1045.2170.

¹H, ¹³C NMR and MALDI-TOF MS spectra

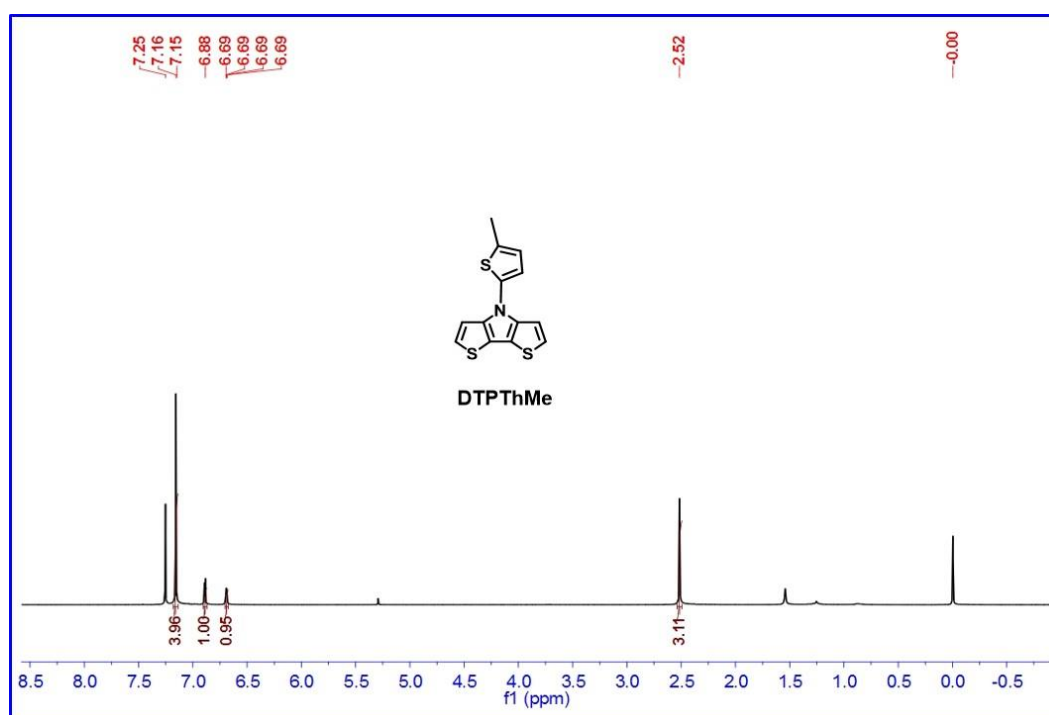


Figure S1. ¹H NMR spectrum of DTPT_hMe.

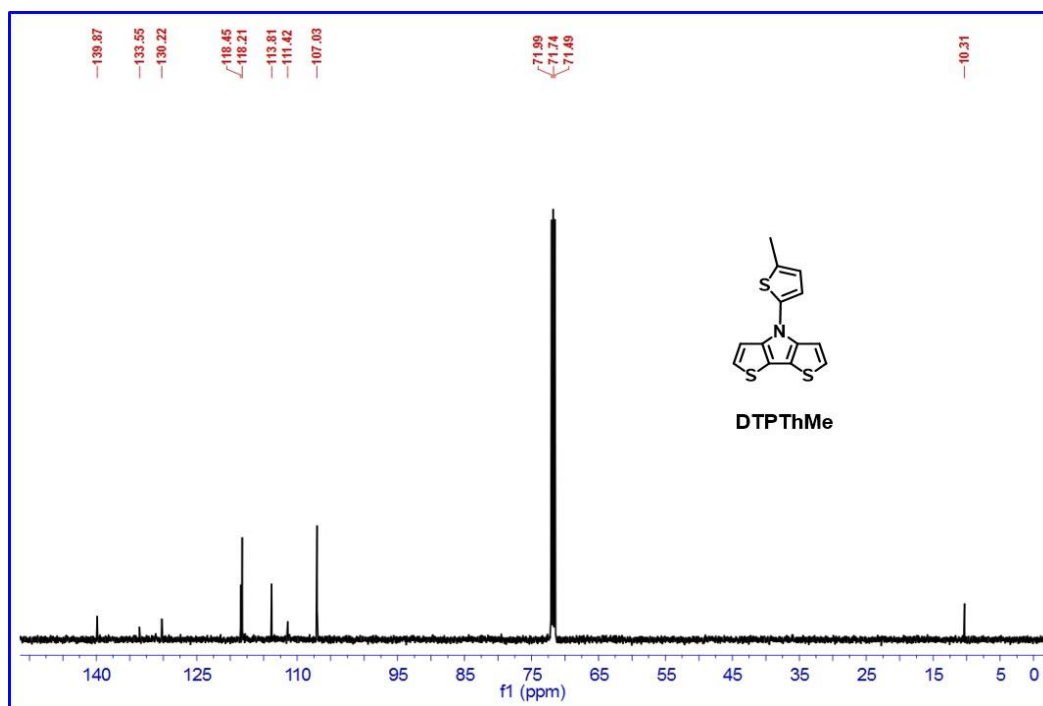


Figure S2. ^{13}C NMR spectrum of DTPThMe.

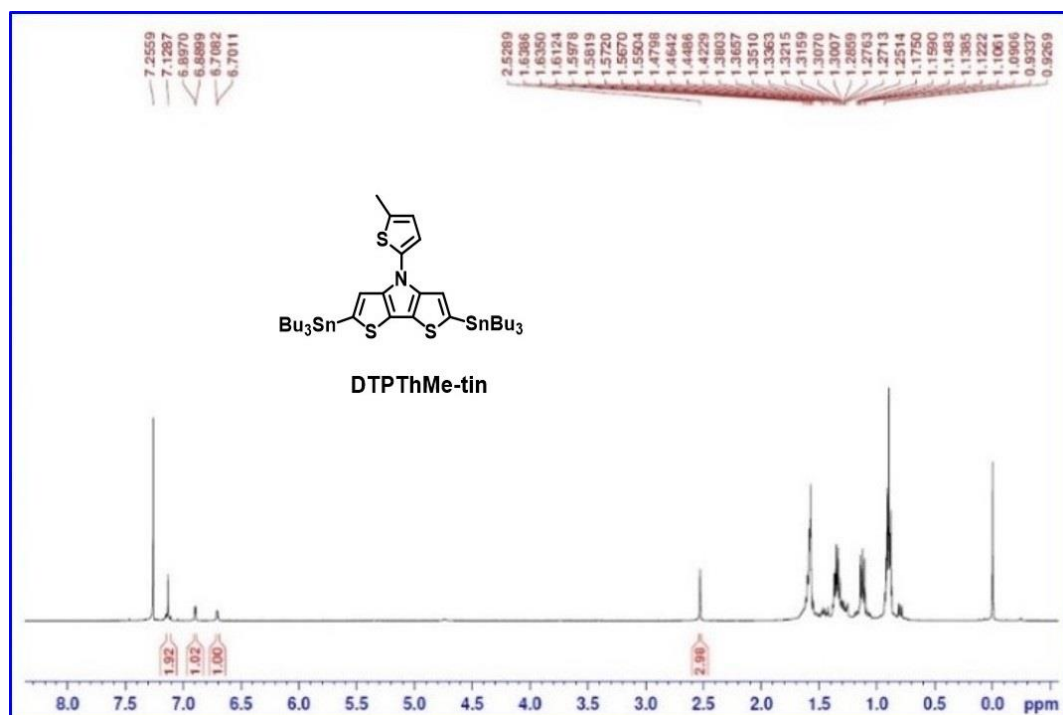


Figure S3. ^1H NMR spectrum of DTPThMe-tin.

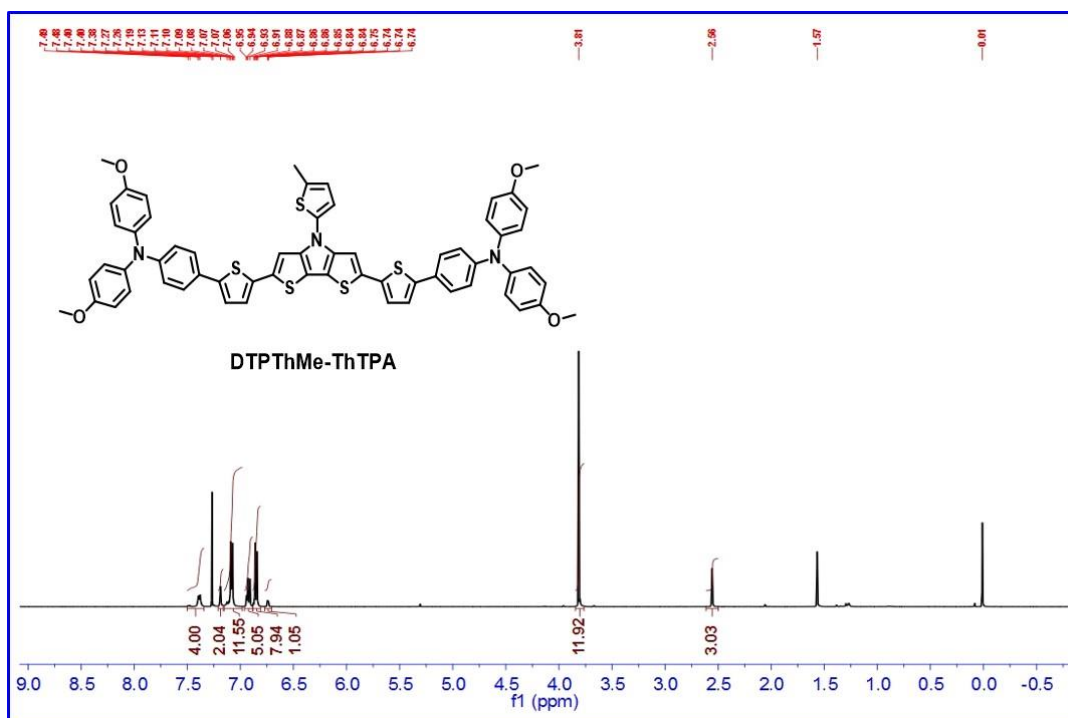


Figure S4. ^1H NMR spectrum of DTPThMe-ThTPA.

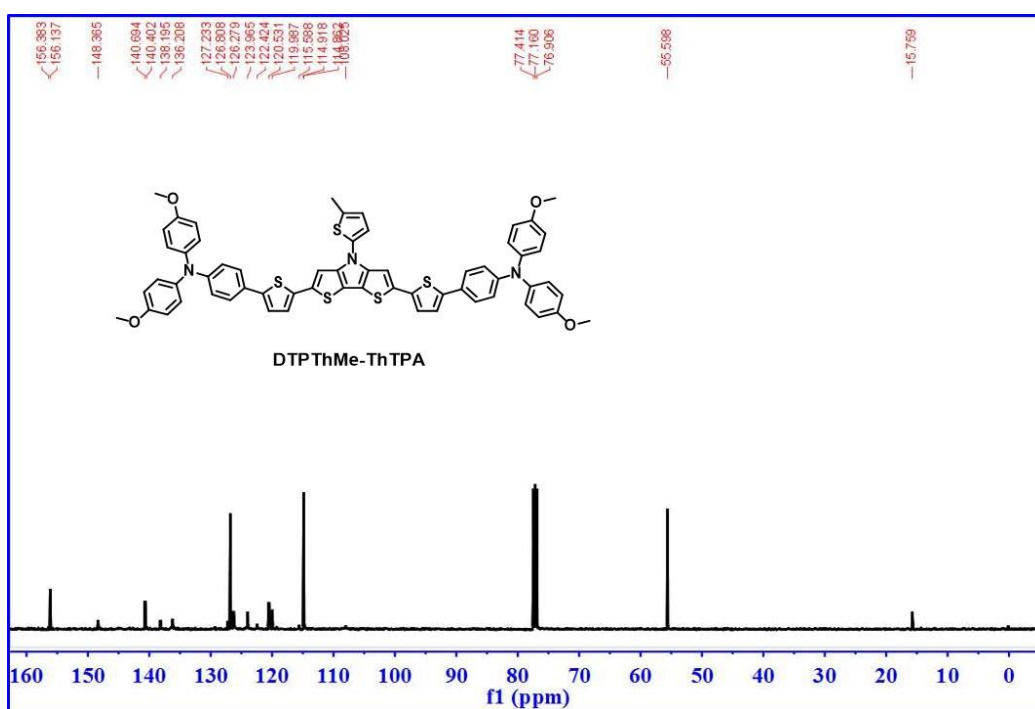


Figure S5. ^{13}C NMR spectrum of DTPThMe-ThTPA.

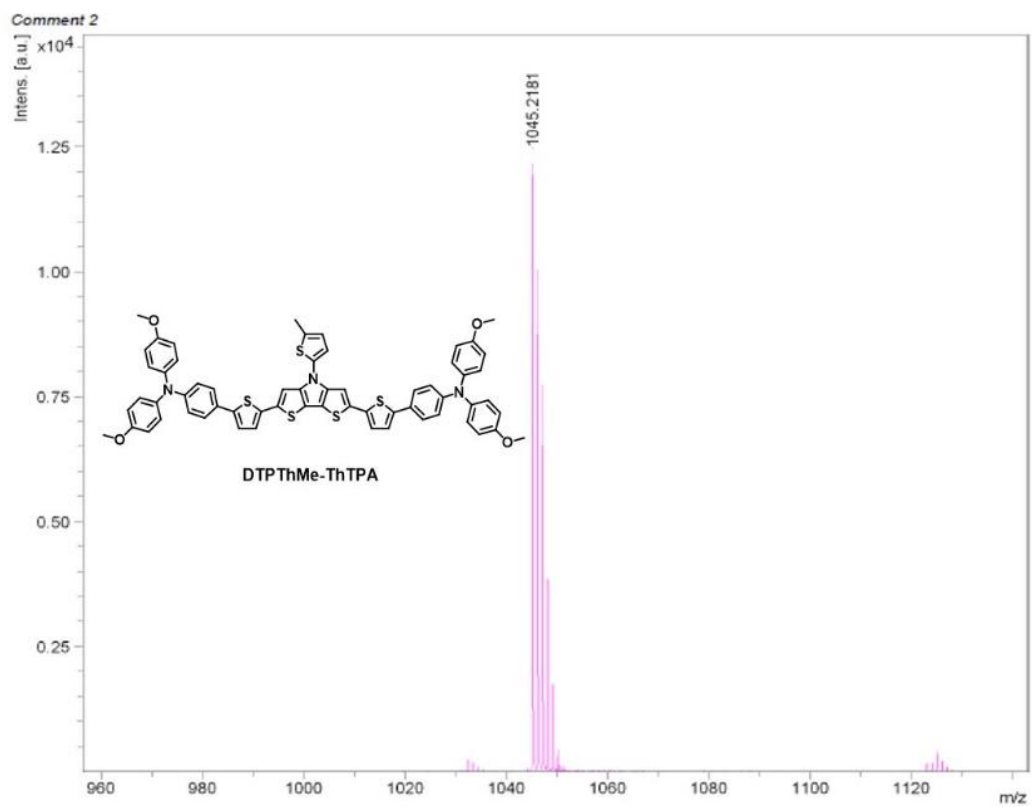


Figure S6. MADLI-TOF mass spectrum for DTPThMe-ThTPA.

EDS Mapping of $\text{Sb}_2(\text{S,Se})_3$

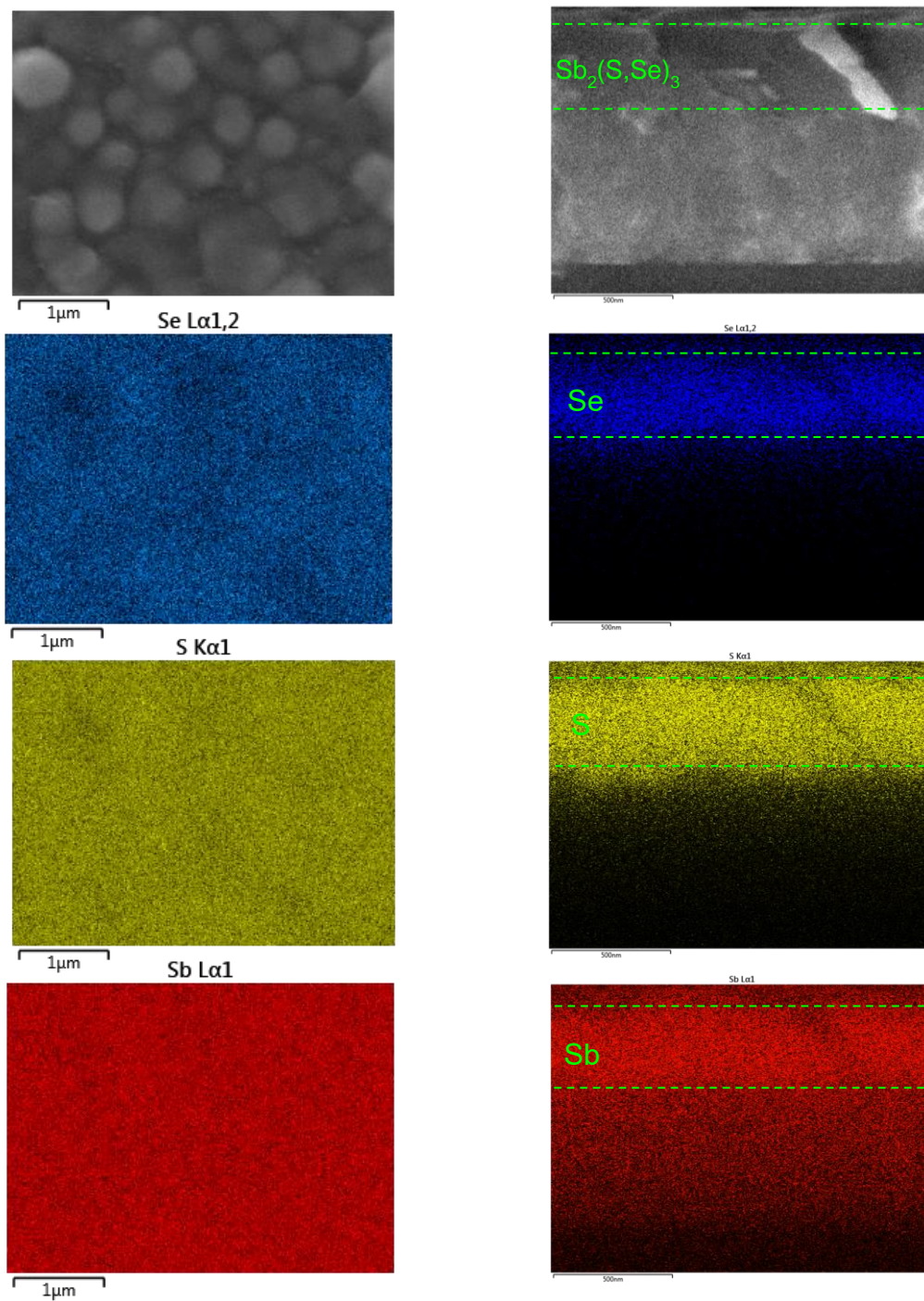


Figure S7. SEM images and EDS elemental mappings (S, Sb, and Se) of $\text{Sb}_2(\text{S,Se})_3$ film (Left: surface; Right: cross-section).

Band energy of $\text{Sb}_2(\text{S,Se})_3$ film

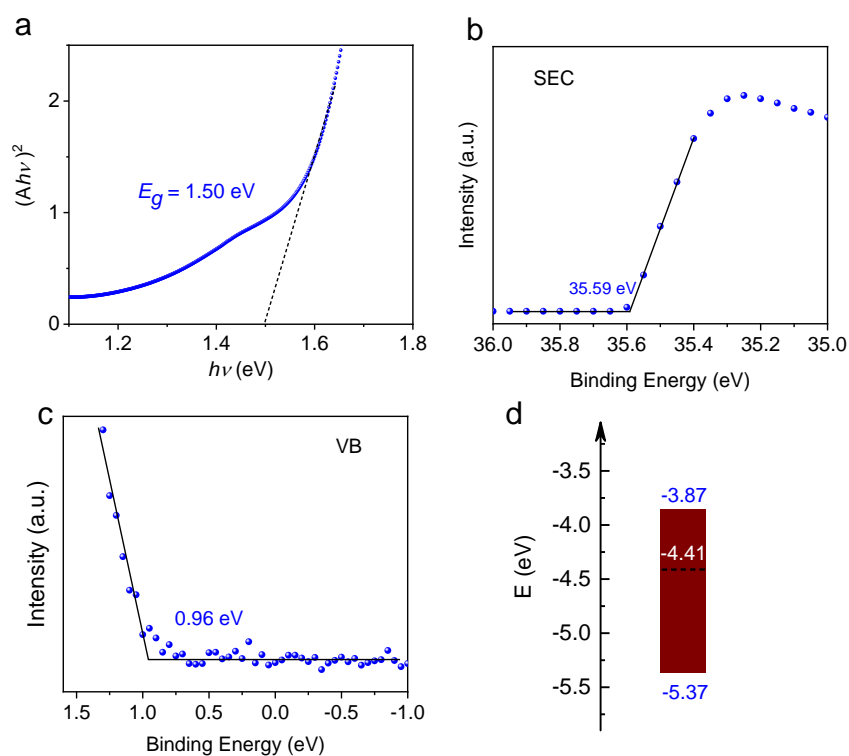


Figure S8. Band energy of $\text{Sb}_2(\text{S,Se})_3$ film. a) $(Ah\nu)^2$ vs energy ($h\nu$) curve and UPS spectra of $\text{Sb}_2(\text{S,Se})_3$ film for b) SEC region, c) VB region. d) Energy diagram of $\text{Sb}_2(\text{S,Se})_3$ film.

DFT calculation

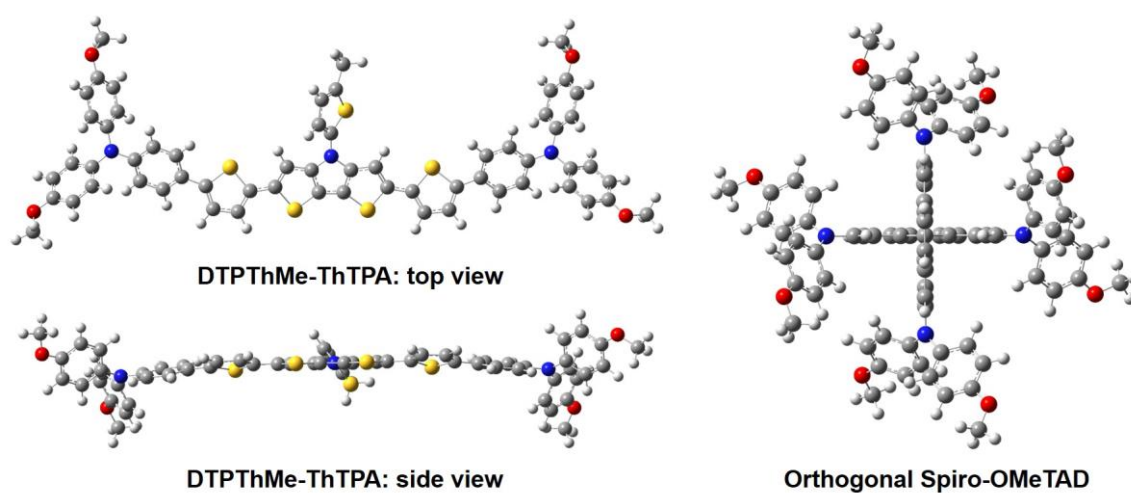


Figure S9. Optimized molecular structures of DTPThMe-ThTPA and Spiro-OMeTAD.

UV-vis absorption spectra

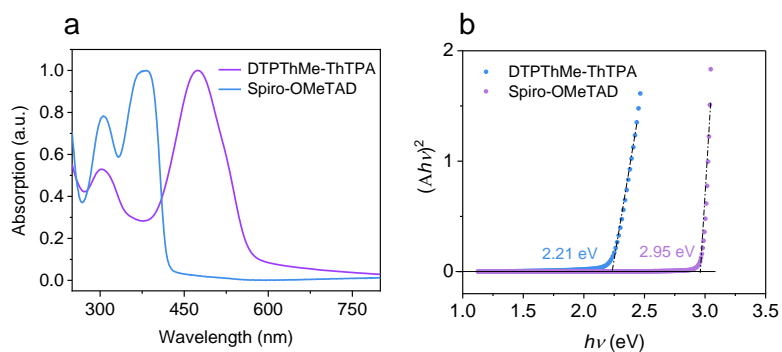


Figure 10. a) UV-vis absorption spectra and b) $(A*hv)^2$ vs energy ($h\nu$) curves of DTPThMe-ThTPA and Spiro-OMeTAD films.

CV measurements

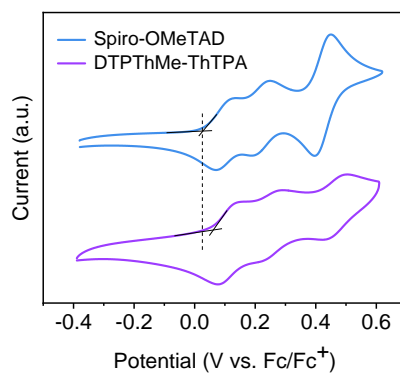


Figure S11. Cyclic voltammograms of DTPThMe-ThTPA and Spiro-OMeTAD in CH_2Cl_2 solutions.

SCLC measurements

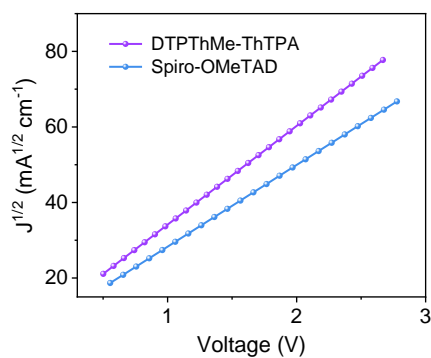


Figure S12. Hole mobility measurements of doped DTPThMe-ThTPA and Spiro-OMeTAD based hole-only devices.

TAS

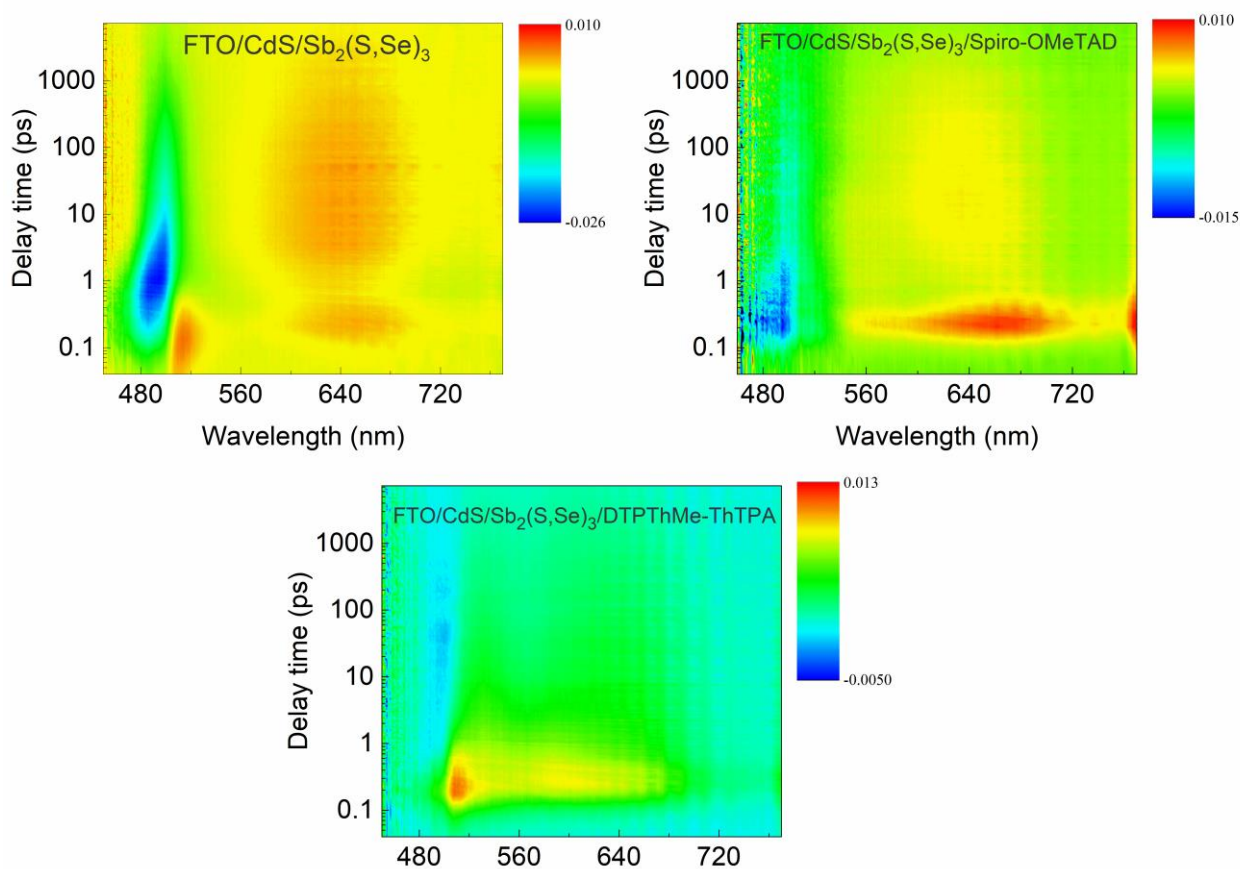


Figure S13. Pseudo-color plot transient absorption spectra of FTO/CdS/Sb₂(S,Se)₃, FTO/CdS/Sb₂(S,Se)₃/Spiro-OMeTAD and FTO/CdS/Sb₂(S,Se)₃/DTPThMe-ThTPA after the excitation at 365 nm (27 nJ). Carrier dynamics can be probed by monitoring the kinetics traces at 650 nm.

Raman spectra

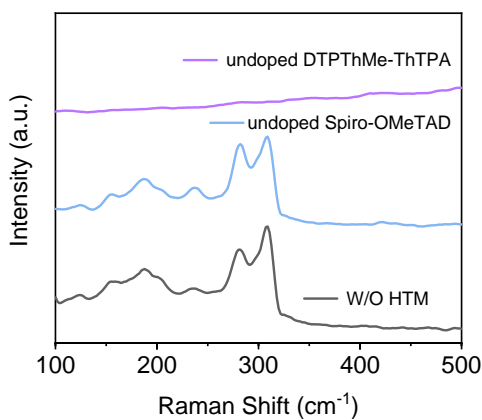


Figure S14. Raman spectra of FTO/CdS/Sb₂(S,Se)₃, FTO/CdS/Sb₂(S,Se)₃/undoped DTPThMe-ThTPA and FTO/CdS/Sb₂(S,Se)₃/undoped Spiro-OMeTAD.

Thermal properties of HTMs

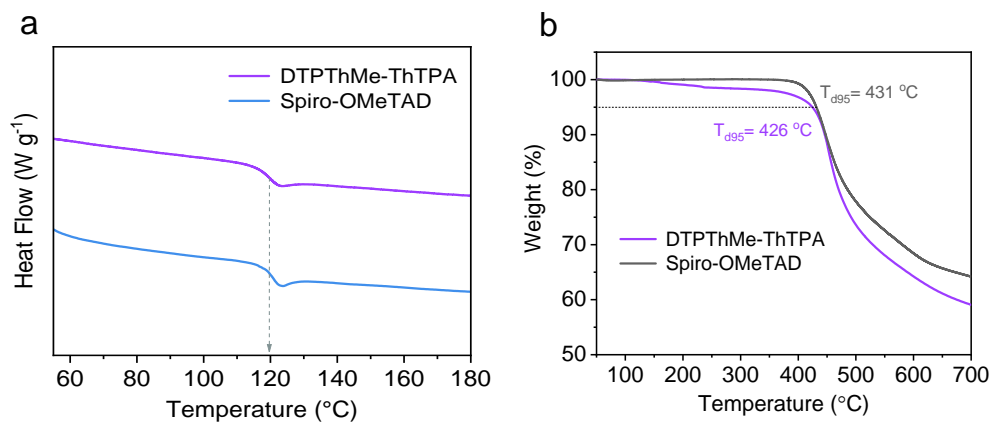


Figure S15. a) Differential scanning calorimetry and b) thermogravimetric thermograms of DTPTThMe-ThTPA and Spiro-OMeTAD.

Efficiency variation for different-concentration DTPTThMe-ThTPA

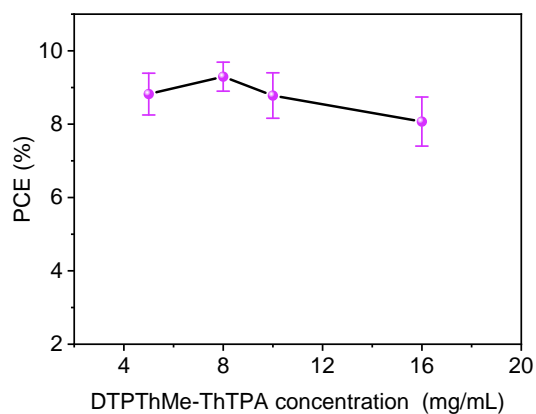


Figure S16. Variation of efficiency for $\text{Sb}_2(\text{S,Se})_3$ solar cells with different concentrations of DTPTThMe-ThTPA HTM.

Device Efficiency

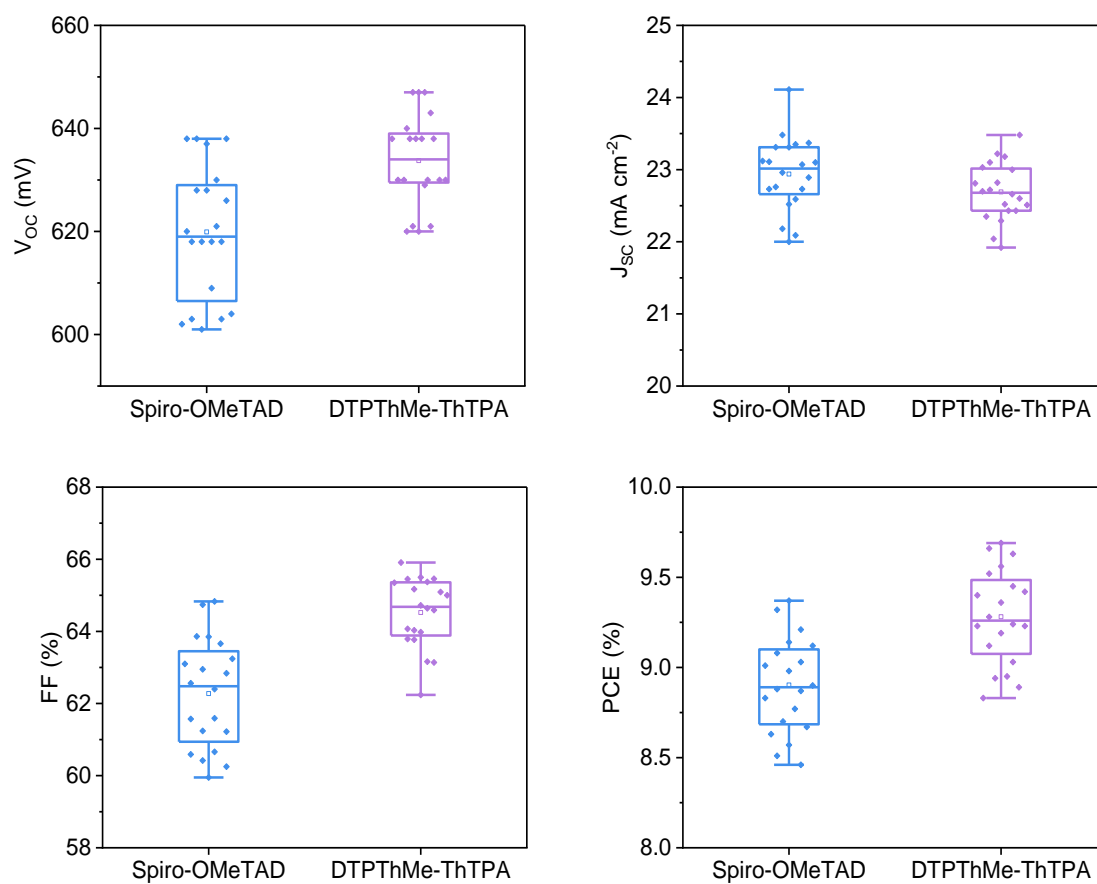


Figure S17. Device performance statistics for $Sb_2(S,Se)_3$ solar cells with Spiro-OMeTAD or DTPTThMe-ThTPA HTMs (20 individual devices for each batch).

Cost for the synthesis of DTPThMe-ThTPA

Table S1. Materials quantities and cost for the synthesis of DTPThMe-ThTPA.

Chemical	Dosage (g)	Price (\$/Kg)	Chemical cost (\$)
DTP	0.5	17700	22.13
2-methyl-5-iodothiophene	0.937	14691	34.21
Cu	0.0887	31.18	0.025
Cs ₂ CO ₃	2.73	392	2.67
CH ₃ CN	35	34.7	2.21
MgSO ₄	3	8.77	0.03
Petroleum ether	300	3.04	0.9
Dichloromethane	120	1.75	.021
Silica gel	80	7.54	0.60
DTPThMe	0.9	54760	49.28
n-BuLi	0.46	175	0.076
Bu ₃ SnCl	2.49	157	0.38
tetrahydrofuran	40	7.73	0.52
Petroleum ether	90	3.04	0.27
DTPThMe-tin	0.525	18110	0.008
ThTPA-Br	0.71	4110 ^a	2.92
Pd(PPh ₃) ₄	0.07	5054	0.3
Toluene	15	6.65	0.1
MgSO ₄	1	8.77	0.008
Petroleum ether	400	3.04	1.2
Silica gel	100	7.54	0.007
Ethyl acetate	1600	1.75	2.6
DTPThMe-ThTPA		About 20 \$/g	

Physical properties of HTMs

Table S2. Optical, electrochemical, thermal, and charge transport properties of DTPThMe-ThTPA and Spiro-OMeTAD.

HTMs	λ_{\max} (nm)	λ_{onset} (nm)	E_g (eV)	LUMO (eV)	HOMO (eV)	T_g (°C)	T_{d95} (°C)	μ_h (cm ² V ⁻¹ s ⁻¹)
Spiro-OMeTAD	382	420	2.95	-1.87	-4.82	120	431	8.02×10 ⁻⁴
DTPThMe-ThTPA	473	561	2.21	-2.66	-4.87	120	426	1.67×10 ⁻³

EIS parameters, V_{bi} , and photocurrent decay time

Table S3. EIS parameters, photocurrent decay time ($\tau_{transport}$) and V_{bi} of W/O HTM, Spiro-OMeTAD, and DTPTThMe-ThTPA devices.

HTMs	R_s (Ω)	R_{rec} (Ω)	$\tau_{transport}$ (μs)	V_{bi} (V)
W/O HTM	24.67	410	9.6	0.54
Spiro-OMeTAD	18.89	771	7.5	0.65
DTPTThMe-ThTPA	16.46	1010	6.6	0.67

Device stability test

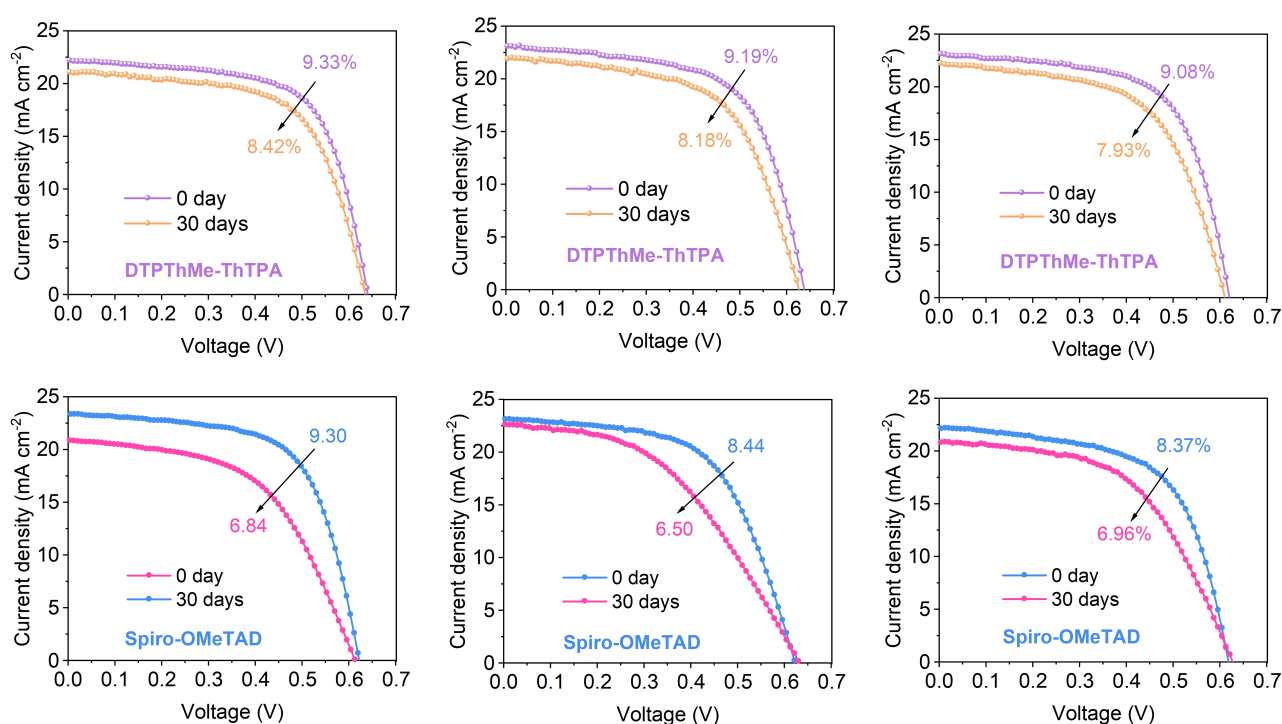


Figure S18. The J - V curves of the DTPTThMe-ThTPA (top) and Spiro-OMeTAD (bottom) devices measured at the beginning and after storage in ambient air for 30 days.

Table S4. Device performances of Spiro-OMeTAD and DTPTThMe-ThTPA devices measured at the beginning and after storage in ambient air for 30 days.

Time	DTPTThMe-ThTPA			Spiro-OMeTAD		
Initial	9.33%	9.19%	9.08%	9.30%	8.44%	8.37%
A month later	8.42%	8.18%	7.93%	6.84%	6.50%	6.96%
Stability Rate ($PCE_{after\ 30\ days}/PCE_{initial}$)	90.25%	89.01%	87.33%	73.55%	77.01%	83.15%

References

1. C. Wu, C. Jiang, X. Wang, H. Ding, H. Ju, L. Zhang, T. Chen and C. Zhu, *ACS Appl Mater Interfaces*, 2019, **11**, 3207-3213.
2. X. Wen, C. Chen, S. Lu, K. Li, R. Kondrotas, Y. Zhao, W. Chen, L. Gao, C. Wang, J. Zhang, G. Niu and J. Tang, *Nat Commun*, 2018, **9**, 2179.
3. C. Jiang, R. Tang, X. Wang, H. Ju, G. Chen and T. Chen, *Solar RRL*, 2018, **3**, 1800272-1800280.
4. W. Hu, W. Zhou, X. Lei, P. Zhou, M. Zhang, T. Chen, H. Zeng, J. Zhu, S. Dai, S. Yang and S. Yang, *Advanced Materials*, 2019, **0**, 1806095.
5. H. Deng, S. Yuan, X. Yang, J. Zhang, J. Khan, Y. Zhao, M. Ishaq, W. Ye, Y. B. Cheng and H. Song, *Progress in Photovoltaics: Research and Applications*, 2018, **26**, 281-290.
6. C. Jiang, J. Yao, P. Huang, R. Tang, X. Wang, X. Lei, H. Zeng, S. Chang, H. Zhong, H. Yao, C. Zhu and T. Chen, *Cell Reports Physical Science*, 2020, **1**, 100001.
7. J. Duan, Y. Zhao, B. He and Q. Tang, *Small*, 2018, DOI: 10.1002/smll.201704443, e1704443.
8. W. Ke, P. Priyanka, S. Vegiraju, C. C. Stoumpos, I. Spanopoulos, C. M. M. Soe, T. J. Marks, M. C. Chen and M. G. Kanatzidis, *J Am Chem Soc*, 2018, **140**, 388-393.